Impact of the Surrounding Network on the Si-O Bond-Breakage Energetics

S.E. Tyaginov[1,2], V. Sverdlov[3], W. Gös[1], Ph. Schwaha[3], R. Heinzl[3], F. Stimpfl[3], T. Grasser[1]
[(1)]Christian Doppler Laboratory for TCAD at the [(3)]Institute for Microelectronics, TU Wien, Gußhausstraße 25-29, A-1040 Vienna, Austria,
[(2)] Ioffe Physico-Technical Institute, 26 Polytechnicheskaya Str., 194021 St.-Petersburg, Russia
phone: +43-1-58801-36025; fax: +43-1-58801-36099; e-mail: tyaginov@iue.tuwien.ac.at

ABSTRACT

We extend the McPherson Model for silicon-oxygen bond-breakage derived for a single SiO_4 tetrahedron to capture the influence of the whole lattice. Several pair-wise potentials have been compared in the model including Mie-Grüneisen as well as diverse forms of TTAM/BKS. The contribution of the whole lattice substantially increases the activation energy for the Si-O bond rupture. The corresponding small transition rate of a non-distorted Si-O bond suggests that the interaction with the electric field alone can not be responsible for the bond-breakage and the contribution of other components such as energy delivered by particles and/or bond weakening is required.

INTRODUCTION

The energetics of the Si-O bond-breakage is one of the most crucial issues in the field of reliability of SiO2 films, especially in the context of Hot-Carrier-Injection (HCI) related degradation and the Time-Dependent-Dielectric-Breakdown (TDDB) [1-7]. There is still no consensus on whether the interaction of the dipole moment with the electric field or the energy delivered by particles is the driving force behind Si-O rupture in silica. As a consequence, several contradicting models based on one of the two main concepts exist: (i) the Thermo-Chemical Model [5,6] claiming that the applied field is responsible for bond-breakage, (ii) the Anode Hole Injection [2,7] and the Anode Hydrogen Release [8] models link Si-O breakage with the energy deposited by particles. All of these models have their shortcomings and a comprehensive model describing Si-O bond-breakage energetics is urgently needed.

A recently proposed model for Si-O rupture – the McPherson Model (MM) [5,6] – calculates the bond-breakage energy using a single SiO_4 tetrahedron. An introduction of the whole lattice substantially changes the picture and the initial MM should be extended in a manner to capture the lattice contribution to the Si-O energetics. Such a model will be designated hereafter as Extended McPherson Model (EMM). For description of interatomic interactions among the Mie-Grüneisen Potential (MGP) [5] other pair-wise potentials – namely TTAM and BKS [9,10] – are also employed. We show that all the potentials exhibit similar Si-O bond-breakage energetics.

PAIR-WISE POTENTIALS

In the original MM the Si-O binding potential has been described in terms of the MGP, i.e. $\Phi_{SiO}(r_{SiO}) = \Phi_B(A_9(r_0/r)^9 - A_2(r_0/r)^2 - A_1(r_0/r))$ with r_{SiO} being the distance between the Si and O ions, Φ_B and r_0 the bond strength and length [5]. To consider the effect of the whole lattice on

the bond energetics one has to capture not only Si-O, but also Si-Si and O-O interactions. We generalize the MGP in the following way:

$$\Phi_{ij}(r_{ij}) = Q_i^{(9)} Q_j^{(9)} r_{ij}^{-9} - Q_i^{(2)} Q_j^{(2)} r_{ij}^{-2} - Q_i^{(1)} Q_j^{(1)} r_{ij}^{-1}, \quad (1)$$

where i and j enumerate the atoms in the lattice, r_{ij} is the interatomic distance, and $Q_i^{(m)}$ are the "effective charges" corresponding to the term of the m-th order.

In general we have 6 independent constants. However, the condition of the electrostatic energy convergence, i.e. convergence of such sums [11]:

$$U^{(m)} = \frac{1}{2} \sum_{n_1,n_2,n_3} \sum_i \sum_j \frac{Q_i^{(m)} Q_j^{(m)}}{|\vec{r}_i - \vec{r}_j + \vec{n}|^m} \quad (2)$$

leads to the electrical neutrality of a structural unit consisting of 6 O and 3 Si atoms. (Indexes i and j enumerate atoms in one primitive cell; $\boldsymbol{n} = n_1\mathbf{a}_1 + n_2\mathbf{a}_2 + n_3\mathbf{a}_3$ with $\mathbf{a}_1$, $\mathbf{a}_2$, $\mathbf{a}_3$ being basis translation vectors; the term with $i = j$ and $\boldsymbol{n} = \mathbf{0}$ is omitted) Thus, $Q_{Si}^{(m)} = -2Q_O^{(m)}$, and only 3 independents constants remain. These parameters may be found by calibration to material properties such as elastic constants and/or cohesion energy. An alternative approach is to calibrate to data obtained with DFT/MD. In this work we follow a more straightforward way and employ commonly-accepted TTAM and BKS potentials constructed just in the manner to mimic DFT/MD results [9,10].

Various forms of TTAM/BKS potentials have the same functional form:

$$\Phi_{ij}(r_{ij}) = kQ_iQ_j / r_{ij} + \alpha_{ij} e^{-\beta_{ij} r_{ij}} - \gamma_{ij} / r_{ij}^6 \quad (3)$$

differing only in the coefficients α_{ij}, β_{ij}, γ_{ij}, e.g. BKS [10,12] and Z1-TTAM [13] ignore Si-Si interaction. (The constant $k \approx 14.402$ converts e^2Å^{-1} into eV.) In the EMM only versions of TTAM/BKS with the "traditional" values of effective charges $Q_{Si}/Q_O = +2.4/-1.2$ in Coulombic term have been employed. Among initial versions of TTAM and BKS the Z1-TTAM and the FB-TTAM are used [12,13].

The potential acting on the Si ion from the rest of the crystal calculated with various forms of TTAM/BKS for the direction from the Si EP perpendicular to the O_3 plane (similar to MM, figure 1a, inset) is depicted in Fig. 1a. All the potentials display the energy minimum corresponding to the EP of the Si ion as well as a singularity at $r = 1.7$ Å due to the presence of the O ion. In all cases the potential profiles do not feature any ledges/saddle points in the direction assumed in the MM. This is due to the effect of the surrounding network, primarily, due to neighboring Si ions which have effective charges twice larger than O and are situated at the distance of ~ 3.2 Å from the Si EP.

To find a secondary minimum other directions have been examined and the saddle point in the direction connecting the Si EP and the middle of the O-O segment (figure1b, inset) has been revealed for all employed pair-wise potentials (figure 1b). The secondary minimum is situated outside the "initial" SiO_4 tetrahedron and the transition of the silicon ion from the 4-fold to the 3-fold coordinated position is interpreted as the breakage of the initial SiO_4 bonding configuration followed by the formation of a Si-Si bridge. The energy barrier separating the

primary and the secondary minima is rather high ~6 eV, steming from a positive contribution to the potential from neighboring Si atoms. *Such a high activation energy suggests that bond-breakage only by the interaction of dipole moment with an electric field is rather unlikely.*

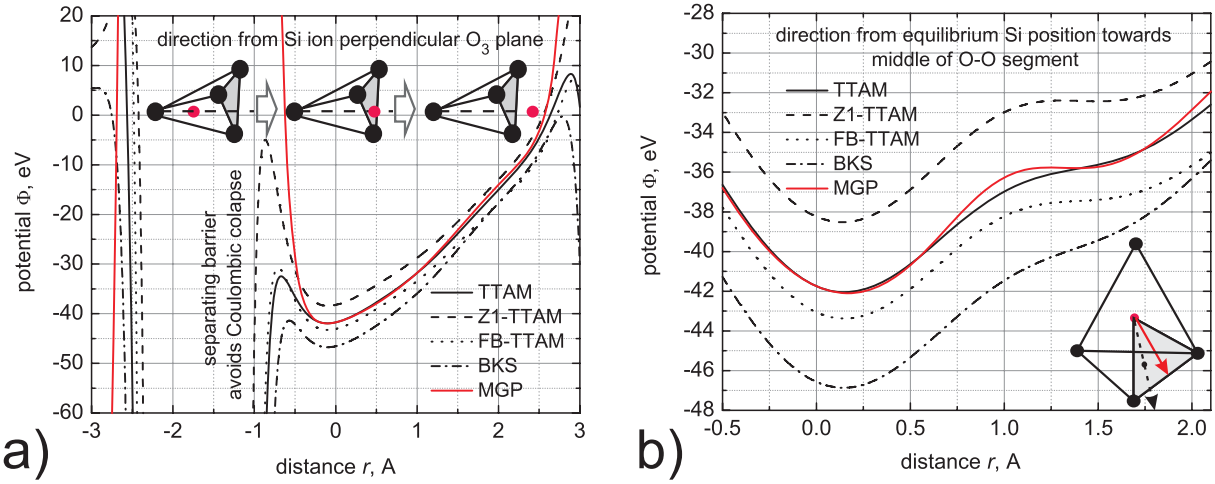

Figure 1. Potential acting on the Si ion from the rest of the crystal as a function of the ion displacement. (a) The displacement is in the direction from the Si EP perpendicular to the O_3 plane (MM direction; sketched in inset); (b) the direction from the Si EP towards the middle of the O-O segment (inset: MM direction is represented by the black arrow; EMM is by the red one).

In order to find "effective charges" $Q_{Si}^{(m)}/Q_O^{(m)}$ we calibrated the MGP-based potential (1) in a manner to represent minima in energy corresponding to the EP of Si and O ions (calculated using TTAM) as well as the cohesion energy of α-SiO_2 lying in the range of 18.6-20.0 eV/formula unit [14-16] (we used 19.1 eV/formula unit, [15]). We obtained: $Q_{Si}^{(1)}Q_O^{(1)} = -41.308$ eV·Å, $Q_{Si}^{(2)}Q_O^{(2)} = -3.148$ eV·Å^2 and $Q_{Si}^{(9)}Q_O^{(9)} = 99.480$ eV·Å^9. For comparison, in the original MM the following set of parameters has been used: $Q_{Si}^{(1)}Q_O^{(1)} = -6.523$ eV·Å, $Q_{Si}^{(2)}Q_O^{(2)} = -7.392$ eV·Å^2 and $Q_{Si}^{(9)}Q_O^{(9)} = 117.964$ eV·Å^9 [5]. We intentionally did not involve the saddle point into the calibration scheme in order to reveal (or not) its existence independently. As shown in figure 1b the secondary minimum exists at the same position as in the case of TTAM/BKS potentials (with a similar energy barrier between minima), moreover, no features in the MM direction have been observed.

BOND-BREAKAGE RATE: EFFECT OF ELECTRIC FIELD AND HOLE CAPTURE

The contribution to the potential due to the interaction of the dipole moment ***p*** with the electric field ***F*** is calculated as:

$$\Phi_{dip}(\vec{r}) = -\vec{p}\cdot\vec{F} = -2e\left[\sum_{i=1}^{4} f_i^*(\vec{r}-\vec{r}_i)\right]\left(\frac{2+\varepsilon}{3}\right)\vec{F}\,, \qquad (4)$$

where the summation is undertaken over 4 oxygen atoms (on positions $\boldsymbol{r}_i$) bonded to the Si ion with the corresponding bond polarity f_i^*; ε = 3.9 is the permittivity of the silica.

The transformation of the MGP-based potential profile for the Si-O bond weakened by hole capture (HC) is depicted in figure 2. The primary and the secondary minima become degenerate at $F_d \sim 5$ MV/cm (cf. with the $F_d \sim 15$ MV/cm obtained in MM [5] which seems too high, because the dielectric strength of silica is substantially lower, i.e. 10 MV/cm, see e.g. [17]).

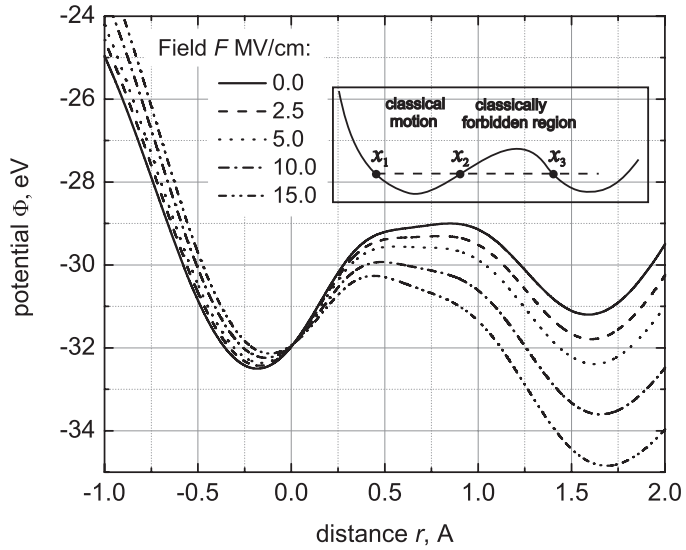

Figure 2. The MGP-based potential profile for the Si-O bond weakened by hole capture with the electric field. The degeneracy of the primary and the secondary minima occurs at $F_d \sim 5$ MV/cm. The inset schematically shows the regions of classically forbidden and allowed ion motion.

The bond-breakage process is considered as a tunneling of a Si ion between the primary and the secondary minima and treated within the WKB approximation. The system of eigenvalues in the quantum well is related to the Si EP (defined by the potential profile $V(x)$) and was calculated according to:

$$\int_{x_1}^{x_2} \sqrt{2m_{Si}\left(E_n - V(x)\right)}dx = (n+1/2)\pi\hbar\,, \tag{5}$$

where x_1, x_2 are points restricting the classical motion of Si (figure 2, inset), m_{Si} is its mass and E_n is the position of the n-th level with the occupancy $f_n = \exp(-E_n / k_B T) / \sum_n \left[\exp(-E_n / k_B T)\right]$.

The energy as a function of level number is shown in figure 3, left inset. The quantum well of the primary minimum becomes shallower with F and the total number of states reduces. The allez-retour time and the probability for tunneling from E_n into the secondary minimum are:

$$\tau_{a-r,n} = 2\sqrt{\frac{m_{Si}}{2}}\int_{x_1}^{x_2} \frac{dx}{\sqrt{E_n - V(x)}} \tag{6}$$

$$T_n = \exp\left(-\frac{2}{\hbar} \int_{x_2}^{x_3} \sqrt{2m_{Si}\left[V(x) - E_n\right]}\, dx \right), \tag{7}$$

where x_2 and x_3 are boundaries for the classically prohibited motion of Si. Multiplying the tunnel probability T_n with the number of particles f_n and the attempt frequency $1/\tau_{a\text{-}r,n}$ one obtains the tunnel rate $P_n = f_n T_n / \tau_{a\text{-}r,n}$ plotted vs. F in the right inset of figure 3. Since tunneling occurs only from levels situated above the bottom of the secondary minimum, the offset of tunneling is pronounced. The cumulative transmission rate P vs. F is plotted in figure 3. The change of slope at $F \sim 5$ MV/cm is related to the involvement of all levels into tunneling. For comparison, P calculated within the MM [6] for a "virgin" Si-O bond is depicted in the same graph (we borrowed the tunnel probability from figure 7 in Ref. [6] and multiplied it by the attempt rate $\nu \sim 10^{13}$ s^{-1} [6]).

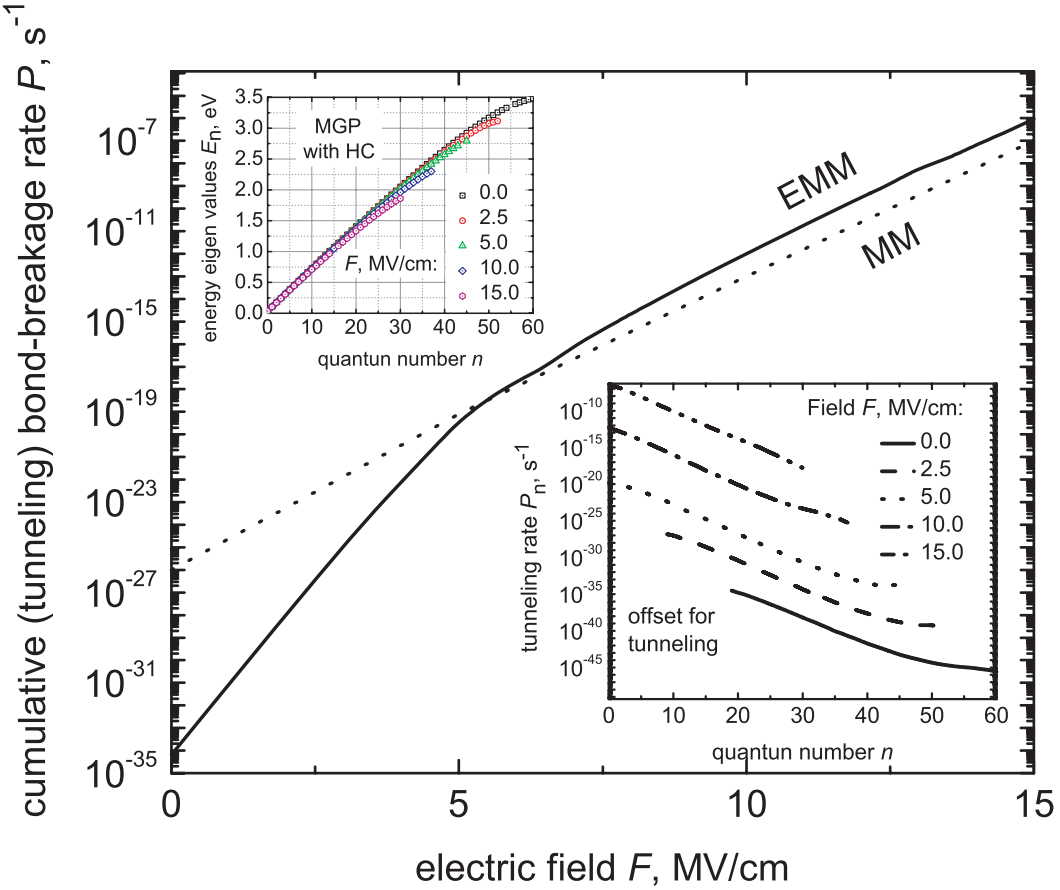

Figure 3. Cumulative bond-breakage rate as a function of the applied field calculated within the MM for a "virgin bond" and within the EMM for a bond weakened by HC. Left inset: the system of energy levels in the quantum well of the primary minimum plotted for different fields. Right inset: tunneling rate vs. level number obtained for various F.

A difference within 3-4 orders of magnitude observed in the wide range of electric field (2.5…15.0 MV/cm) for fundamentally different scenarios (with/without HC) reflects the strong effect of the surrounding network on the Si-O bond energetics. The contribution of the neighboring Si atoms not only changes the position of the secondary minimum but enlarges the

activation energy for bond-breakage and, hence, abruptly diminishes the probability of bond rupture. In the EMM a considerable rate for transmission of the Si from 4-fold coordination to the 3-fold one is achieved only if the bond is weakened (e.g. by HC). This suggests that the electric field alone cannot trigger the breakage process. These considerations thus require the contribution of another mechanism to the bond-breakage. For example, one may envisage bond weakening by HC, O-Si-O/Si-O-Si bond angle variations, build up of bond strain (typical for the Si/SiO_2 interface) or another structural disorder. Another important contribution to the tunneling rate results from the excitation of the Si ion into higher levels characterized with higher barrier transparency due to the energy transferred from energetic particles, i.e. hot carriers and/or mobile hydrogen and its species.

CONCLUSION

To summarize, an extension of the initial McPherson Model in order to capture the effect of the whole lattice on Si-O bond energetics has been investigated. The secondary minimum is revealed in a different position compared to the MM and the activation energy for the transition of the Si ion from the 4-fold to the 3-fold position is rather high. The surrounding lattice stabilizes the SiO_4 tetrahedron, making the bond rupture mechanism suggested by McPherson certainly unlikely. Our results demonstrate that only the common action of the dipole – electric field interaction and other factors such as bond weakening and/or energy delivered by particles can trigger the breakage mechanism.

REFERENCES

1. D. Saha, D. Varghese, and S. Mahapatra, *IEEE Electron Dev. Lett.* **EDL-27**, 585 (2006).
2. S. Mahapatra, D. Saha, D. Varghese, P.B. Kumar, *IEEE Trans. Electron Dev*. **ED-53**, 1583 (2006).
3. T.-Ch. Yang, C. Saraswat, *IEEE Trans. Electron Dev.* **ED-47**, 746 (2000).
4. G.S. Ristis, *J. Phys. D: Appl. Phys.* **41**, pap. No. 023001 (2008).
5. J.W. McPherson, *J. Appl. Phys.* **99**, pap. No. 083501 (2006).
6. J.W. McPherson, *45th Annual Intern. Reliab. Phys. Symp.*, 209 (2007).
7. M. Alam, J. Bude, A, Ghetti, *38th Annual Intern. Reliab. Phys. Symp.*, p. 21 (2000).
8. D.J. DiMaria, *J. Appl. Phys.* **87**, 8707 (2000).
9. S. Tsuneyuki, M. Tsukada, H. Aoki, Y. Matsui, *Phys. Rev. Lett*. **61**, 869 (1998).
10. B.W.H. van Beest, G.J. Kramer, R.A. van Santen, *Phys. Rev. Lett*. **64**, 1955 (1998).
11. U. Essmann, L. Perera, L. Berkowitz, T. Darden, H. Lee, L.G. Pedersen, *J. Chem. Phys.* **103**, 8577 (1995).
12. A.R. Al-Derzi, M.G. Gory, K. Runge, S.B. Trickey, *J. Phys. Chem. A* **108**, 11679 (2004).
13. W. Zhu, K. Runge, S.B. Trickey, *J. Comp.-Aid. Mater. Design* **13**, 75 (2006).
14. Tandia, G. Sarrabayrouse, A. Martinez, *Thin Solid Films* **296**, 122 (1997).
15. F. Jollet, C. Noguera, *Phys. Stat. Sol. (b)* **179**, 473 (1993).
16. Sh. Munetoh, T. Motooka, K. Moriguchi, A. Shintani, *Comput. Mat. Sci.* **39**, 334 (2007).
17. S.M. Sze and K.K. Ng, *Physics of Semiconductor Devices*, 3nd edition, W&S, NY, 2006.